UNIVERSITÀ DEGLI STUDI DI PADOVA

Dipartimento di Fisica e Astronomia "Galileo Galilei"

Corso di Laurea in Fisica

Tesi di Laurea

Optimal dynamics of Rydberg atom chains

Dinamiche ottimali di stringhe di atomi di Rydberg

Relatore

Prof. Simone Montangero

Correlatore

Dr. Simone Notarnicola

Laureando

Alberto Schiavinato

Anno Accademico 2022/2023

Abstract

In the context of quantum simulation, one of the main research focuses is the capability of arranging and coherently manipulating large quantum many-body states. Recent experiments are showing an ever-growing improvement in their capabilities, allowing the direct observation of unprecedented quantum phenomena. A prototypical example is given by the realization of so-called "Schrödinger's cat" states, formed by the coherent superposition of two macroscopically different quantum many-body states. This experiment has been recently realized using Rydberg atoms ("Generation and manipulation of Schrödinger cat states in Rydberg atom arrays", Omran et al., Science 365, 570-574 (2019)) [1], which, due to their great versatility, are considered a particularly promising candidate for quantum simulation and computation experiments. In parallel with experimental improvements, several software have been developed to design and optimize the experimental protocols by controlling the experimental platform parameters. In this thesis, by taking inspiration from the aforementioned publication, we use the software Qruise, a commercial optimization platform, to design experimental quantum protocols to generate Greenberger-Horne-Zeilinger (GHZ) states on a one-dimensional Rydberg atoms array.

Nel contesto della simulazione quantistica, uno dei principali focus di ricerca è la capacità di ordinare e manipolare coerentemente grandi stati quantistici a molti corpi. Recenti esperimenti mostrano un sempre crescente miglioramento nelle loro capacità, permettendo l'osservazione diretta di fenomeni quantistici senza precedenti. Un prototipo è dato dalla realizzazione dei cosiddetti "gatti di Schrödinger", stati quantistici formati dalla sovrapposizione coerente di due stati quantistici a molti corpi. Questo esperimento è stato di recente realizzato utilizzando atomi di Rydberg ("Generation and manipulation of Schrödinger cat states in Rydberg atom arrays", Omran et al., Science 365, 570-574 (2019)) [1], i quali, grazie alla loro grande versatilità, sono considerati candidati particolarmente promettenti per esperimenti di computazione e simulazione quantistica. In parallelo con gli sviluppi sperimentali, sono stati sviluppati diversi software per progettare e ottimizzare i protocolli sperimentali controllando i parametri dell'esperimento. In questa tesi, prendendo ispirazione dalla suddetta pubblicazione, usiamo Qruise, un software commerciale di ottimizzazione, per progettare protocolli sperimentali quantistici per generare stati di Greenberger-Horne-Zeilinger (stati GHZ) su una stringa monodimensionale di atomi di Rydberg.

Contents

Acknowledgments

I would like to express my gratitude and respect to my thesis advisors, Simone M. and Simone N., for their invaluable guidance throughout the entire process of making this thesis. Their availability and expertise are much appreciated, and their demanding standards ensured that I would grow proud of this project.

I am also grateful to the Qruise team, particularly Anurag and Marco, for their assistance and support in navigating the software. This thesis is made possible thanks to their invaluable contributions.

A special thanks to those who had the patience to endure me during these academic years:
my family, who still struggle to understand what exactly am I doing at university, but nonetheless offered invaluable support and love;
my friends, who gave me innumerable moments of joy and happiness, and helped me grow into what I now am;
my peers and colleagues, who helped me to keep being motivated, and made much more enjoyable these years of study.
Without you, all of this would not be possible.

Introduction

The central concepts of quantum simulation have their inception in a foundational paper published by Richard Feynman in the early '80s, which defines a quantum simulator and explores why it is necessary to advance in science research [2].

Feynman envisioned the potential of simulating quantum systems using a controllable quantum system itself; however, quantum simulations primarily existed only as theoretical frameworks.

With the advent of sophisticated experimental technologies, including trapped ions [3], Josephson junction-based superconducting circuits [4], and trapped neutral atoms [5, 6], researchers have made unprecedented strides in the realization of these theoretical constructs.

As a consequence, the possibility to perform experiments on quantum simulators allowed the scientific community to consider them as a way to solve several problems that before were deemed to be too challenging to tackle. The defining feature of these problems is that their complexity is exponential, meaning that the number of operations needed to find a solution exponentially increases with the size of the system in study.

These exponentially complex problems range between many disciplines, including math and cryptography (prime numbers factorization) [7], computer science (search algorithms) [8], biology and medicine (biomolecular dynamics) [9], and many more, surpassing, at a certain size, the capabilities of classical computers [10].

Specifically, various quantum phenomena can be difficult to simulate: quantum systems with several components called quantum many-body systems, are represented by a wave function in the Hilbert space, whose size scales exponentially. If a state is not separable, namely it is entangled, a complete description of the system requires the knowledge of the whole wave function.

Quantum simulators are considered a powerful tool to respond to these requirements because they harness the advantages offered by quantum mechanics, which can be used to replicate and simulate complex dynamics.

In the current scenario, quantum simulators have demonstrated their prowess in tackling complex problems such as quantum many-body systems. Superconducting qubits [11], trapped ions [12] and Rydberg atoms already have displayed impressive capability at meeting theoretical requirements to perform operations and state manipulation.

On the one hand, these well-established technologies are considered by many to be the most favored candidates to be the basis of future hardware, on the other hand they struggle to maintain both coherence and entanglement for a useful amount of time.

Notably, experimental platforms such as arrays of optically trapped Rydberg atoms have showcased promising results, bridging the gap between theoretical conjecture and tangible experimental observations. Quantum many-body systems' complexity is largely caused by the exponential rise of the state space dimension: Rydberg atoms have proven successful for many-body quantum state engineering due to their strong state-dependent interactions [13].

To better study this experimental scenario, software to perform classical numerical simulation of physical systems proves to be an important resource: they constitute a convenient

benchmark to test theoretical models and design experimental setups.

In this thesis, we focused on studying and virtually replicating a smaller-scale version of an experiment where Rydberg atom chains are implemented to explore many-body phenomena on a quantum simulator [14].

For this task, we chose to use Qruise, a commercially available software.

Qruise offers both a Cloud Integrated Development Environment (CIDE) and a vast library of methods and classes useful for setting up a virtual experimental setup. Furthermore, the software can reliably and quickly allow us to explore dynamics by acting on parameters, and extract useful information like state amplitudes, populations, and many more data to aid the user in designing and performing experiments.

The thesis is organized as follows:

- In chapter 1, we present a theoretical introduction to the system, describe Rydberg atoms both as a single system and in an array, and explain how qubits can be encoded in this system. Then we describe the experimental implementation of the system, focusing more on the essential components needed to construct the effective Hamiltonian of the atom array.

- In chapter 2, we discuss how Qruise simulates Rydberg atom arrays. We describe its main features, as well as the packages the software provides to facilitate the simulated implementation of experimental components. We also explore Qruise's limitations as a simulation software.

- In chapter 3, we present the protocols we simulated. We begin by attempting a simple simulation, to assert the behavior of the system as well as to familiarize ourselves with how the software works. Then we implement a simulation to study specific properties of Rydberg atoms, considering more complex scenarios. Finally, we reproduce a protocol to obtain a Greenberg-Horne-Zeilinger state with up to eight atoms. We assert the difficulty of the task and what solutions can be considered to successfully construct that state on a Rydberg atoms array.

Chapter 1

Rydberg atom platforms

In this chapter, we are going to provide the theoretical and experimental description of Rydberg atoms.

First, we describe the single-atom platform, specifically the main features of Rydberg atoms, the encoding of qubits on this platform, and its dynamics under a unitary evolution.

Then, we explore how a multi-atomic system behaves, and show how useful properties can be explained and put to use to gain computation advantages from this physical approach. We introduce the concept of Rydberg blockade, which is a fundamental property of this platform, and briefly discuss the parameters that come into play in the preparation of a Greenberger-Horne-Zeilinger state, that is an entangled quantum state involving three or more qubits.

Lastly, we describe the experimental setup that will be virtually simulated by our software, placing greater emphasis on the components that are directly related to qubit manipulation.

1.1 Single Rydberg atom

A Rydberg atom is an excited atom with one or more electrons elevated to a very high principal quantum number n [15]. The energy of an electronic atomic state is, in first approximation[1], determined mainly by the Coulomb interaction between the electron and the nucleus, expressed by the Rydberg formula

$$E_n = -hcR_\infty \frac{Z^2}{n^2}, \tag{1.1}$$

where h is the Planck constant, c the speed of light, R_∞ the Rydberg constant, Z the atomic number and n the principal quantum number. For Rydberg atoms, the value of n can be larger than typical excited atomic states, which means that the electron is far from the nucleus[2]. In this condition, several peculiar properties arise; most notably the atom responds exaggeratedly to external electromagnetic fields, its size is orders of magnitude larger than unexcited atoms of the same species, and this excited state has a particularly long decay time (of the order of 150μs for the 70S state of Rb atoms) [1].

There are various ways to encode qubits on Rydberg atoms [16], depending on the properties we want for our system: one possible implementation is to use the atomic ground state $|g\rangle$ to represent the $|0\rangle$ state from computational basis, and a highly excited Rydberg state $|r\rangle$ as the $|1\rangle$ state. Typically the excited state's principal quantum number is in the range of $n = 60 - 80$.

[1] This formula correctly predicts energy levels of hydrogen-like atoms, but it is approximate for more-than-one-proton nuclei. In any case, it generally constitutes the most predominant term.

[2] Not every atom can be a good Rydberg atom: when too excited, some atomic species can undergo ionization, due to the electron's transition to a not anymore bounded state.

Single qubit manipulation can be performed via monochromatic fields carried by lasers, that realize the Hamiltonian

$$\hat{H} = \Big(\frac{\Omega(t)}{2}\,|g\rangle\langle r| + h.c.\Big) - \Delta(t)\,|r\rangle\langle r| \tag{1.2}$$

where the states $|g\rangle$ and $|r\rangle$ refer to the atom's ground state and excited Rydberg state, the Rabi frequency $\Omega(t)$ characterizes the strength of the coupling, and $\Delta(t)$ the detuning, acting only on Rydberg states.

The unitary evolution is defined by the propagator

$$U(t) = \exp\big(-i\frac{H}{\hbar}t\big), \tag{1.3}$$

We want to show the effect of the driving terms proportional to Ω. We set $\Delta = 0$, thus the Hamiltonian simplifies to

$$\frac{H}{\hbar} = \frac{\Omega(t)}{2}\sigma_x, \tag{1.4}$$

where $\sigma_x = \begin{pmatrix} 0 & 1 \\ 1 & 0 \end{pmatrix}$ is the $\hat{X}$ Pauli matrix.

If we consider as the initial state a qubit in the state $|0\rangle$, and a drive pulse with constant frequency $\Omega(t) = \Omega$, the propagator takes the form:

$$\begin{aligned} U(t) &= \exp\!\left(-i\frac{\Omega t}{2}\sigma_x\right) = \sum_{j=0}^{\infty} \frac{(-i\frac{\Omega t}{2})^j}{j!}(\sigma_x)^j = \\ &= \sum_{k=0}^{\infty} \frac{(-i\frac{\Omega t}{2})^{2k}}{(2k)!}\mathbf{1}_2 + \sum_{m=0}^{\infty} \frac{(-i\frac{\Omega t}{2})^{2m+1}}{(2m+1)!}\sigma_x = \\ &= \cos\!\left(\frac{\Omega t}{2}\right)\mathbf{1}_2 - i\sin\!\left(\frac{\Omega t}{2}\right)\sigma_x. \end{aligned} \tag{1.5}$$

If we want to flip the state $|0\rangle$ into $|1\rangle$ or viceversa, we have to set the gate time T so that $\Omega T = (1/2 + k)\pi$, with $k \in \mathbb{Z}$. This is a simplification: in general, we can define Ω as a function of time, therefore the relation is generalized as

$$\int_0^T \Omega(t)dt = (1/2 + k)\pi. \tag{1.6}$$

1.2 Multi atom arrays and Rydberg blockade

In general, two atoms occupying sites i and j of a lattice interact if excited to a Rydberg state. The interaction Hamiltonian is in the form

$$\hat{H}_{i,j} = V_{i,j}\,|r_i, r_j\rangle\langle r_i, r_j| = \frac{C_6}{R_{i,j}^6}\,|r_i, r_j\rangle\langle r_i, r_j|\,, \tag{1.7}$$

where $|r_i, r_j\rangle \coloneqq |r\rangle_i \otimes |r\rangle_j$ is a pair of Rydberg states of atom i and j respectively, at distance $R_{i,j}$, and $V_{i,j} = \frac{C_6}{R_{i,j}^6}$ is the interaction strength coefficient; $C_6 > 0$ represents the van der Waals coefficient. The van der Waals interactions between the same Rydberg states are repulsive and, since the atoms are excited to S states, isotropic.

Taking these results into account, the dynamics of a Rydberg atom array is governed by the quantum many-body Hamiltonian

$$\frac{H}{\hbar} = \sum_{i=1}^{n} \frac{\Omega}{2}\sigma_x^i - \sum_{i=1}^{n} \Delta n_i + \sum_{i<j} V_{ij} n_i n_j, \tag{1.8}$$

where n is the number of atoms, n_i denotes the projector onto the Rydberg state of the atom i: $n_i \coloneqq |r_i\rangle\langle r_i|$, and $\sigma_x^i(n_i)$ is given by the product

$$\sigma_x^i(n_i) = \mathbf{1}_2 \otimes \cdots \otimes \mathbf{1}_2 \otimes \sigma_x(n_i) \otimes \mathbf{1}_2 \otimes \cdots \otimes \mathbf{1}_2, \tag{1.9}$$

where σ_x is at the position corresponding to the i-th atom. The detuning term Δ acts on single atoms, favoring their excitations.

We can fine-tune the interaction strength by varying the array atoms spacing $R_{i,i+1}$, since intensity scales as $V_{i,i+1} = \frac{C_6}{R_{i,i+1}^6}$. Setting $\Delta = 0$, the Hamiltonian is

$$\frac{H}{\hbar} = \sum_{i=1}^{n} \frac{\Omega}{2}\sigma_x^i + \sum_{i<j} V_{ij} n_i n_j = \sum_{i=1}^{n} \frac{\Omega}{2}\sigma_x^i + \sum_{i<j} \frac{C_6}{R_{i,j}^6} |r_i, r_j\rangle\langle r_i, r_j|, \tag{1.10}$$

where, in our case, $C_6/2\pi = 1725\text{GHz}(\mu\text{m})^6$ and $\Omega/2\pi = 2.5\text{MHz}$

If the array spacing is $a = 15\mu\text{m}$, we measure an interaction strength coefficient of $V_{i,i+1}/2\pi = 0.95\text{MHz}$; in this case, the action of Ω is the predominant effect. However, when atoms are sufficiently close to each other ($a = 5\mu\text{m}$) the Rydberg-Rydberg van der Waals interaction between nearest neighbors $V_{i,i+1}$ greatly exceed the Rabi frequency Ω ($\frac{V_{i,i+1}}{\Omega} \sim 44$), resulting in a suppression of simultaneous excitations of both atoms. This phenomenon is called Rydberg blockade, and it plays a fundamental role in Rydberg atom arrays.

The distance between two neighboring atoms at which this phenomenon appears is called Rydberg blockade radius R_b and is measured by setting $\Omega = V(R_b)$, so that

$$R_b = \left|\frac{C_6}{\Omega}\right|^{1/6}. \tag{1.11}$$

For instance, for $\Omega/2\pi = 2.5$ MHz and $C_6/2\pi = 1725\text{GHz}(\mu\text{m})^6$, we obtain a blockade radius of $R_b = 6.92\mu\text{m}$.

We now focus on the collective behavior of the array; setting the value of Ω at a constant value for all the atoms, and preparing an array in the initial state $|g_1 g_2 \cdots g_n\rangle$ with spacing $a > R_b$, we will observe a simultaneous and collective excitation of all atomic states into the Rydberg state $|r_1 r_2 ... r_n\rangle$, oscillating back at the global ground state $|g_1 g_2 ... g_n\rangle$ at the same frequency as Ω.

However, the system's dynamics change drastically as we decrease the distance between the atoms, specifically when the length of the array is comparable with the blockade radius ($R_{1,n} \sim R_b$): the van der Waals interactions between every atom are now are the dominant terms and exceed the Rabi frequency. As a result, the state oscillates with a frequency Ω_{eff} between the state $|g_1 g_2 ... g_n\rangle$ and a collective state, formed by the coherent superposition of all states with exactly one atom in the Rydberg state: $|\psi_{single}\rangle = \frac{1}{\sqrt{n}}(|r_1 g_2 g_3 ... g_n\rangle + |g_1 r_2 g_3 ... g_n\rangle + ... + |g_1 g_2 g_3 ... r_n\rangle)$.

This oscillation of the probability exhibits an important property: its frequency that we call Ω_{eff} is proportional to the square root of the number of atoms in the array. To see why this happens we have to compute the effect that the first term of the Hamiltonian defined in (1.8) has on the array: applying the ground state to its term results in a summation over all atoms indexes

$$\frac{1}{2}\sum_{i=1}^{n} \Omega\sigma_x^i |00\cdots0\rangle = \frac{1}{2}\Omega_{eff} |\psi_{single}\rangle, \tag{1.12}$$

where $\Omega_{eff} = \sqrt{n}\Omega$; the term $\sqrt{n}$ is thus multiplied to ensure the conservation of vector norm, resulting in an oscillation frequency of the probability of $|\psi_{single}\rangle$ greater than Ω.

We now focus on the evolution of the state $|\psi_g\rangle = |00\cdots0\rangle$, when applying different values of Δ while keeping Ω fixed. At large negative values of Δ/Ω, all atoms of the array are in the $|g\rangle$ state. As Δ/Ω increases toward positive values, excitations are more and more favored, resulting in a growing number of atoms in the $|r\rangle$ state whose interactions are no more negligible. This gives rise to spatially ordered phases, in which atoms follow a regular arrangement of the excitations called Rydberg crystal.

If we set the array spacing such that $V_{i,i+1} \gg \Delta \gg \Omega \gg V_{i,i+2}$ and $a < R_b$, with respect to one atom the nearest neighbor $i+1$ is within the blockade radius, while the next-nearest one has negligible interactions with the first atom i; after completing the sweep from negative to positive values of Δ/Ω, the system corresponds to a Rydberg crystal that exhibits Z_2 translational symmetry, analogously to the transition from a disordered or paramagnetic phase to an antiferromagnetic order in magnetic system. If the spacing is further set to less than the blockade radius so that two or more atoms fit inside the blockade radius of another atom, this procedure gives rise to other translational symmetries: for example, if $V_{i,i+1}, V_{i,i+2} \gg \Delta \gg \Omega \gg V_{i,i+3}$ we obtain an array with Z_3 symmetry, and so on.

To obtain more regular crystalline structures, dynamical and site-specific control of the detuning driving lasers is needed for our array to undergo an adiabatic transition into crystalline states.

Ultimately the implementation of a trapezoidal signal for the Rabi pulse and a linear ramp for the detuning pulse allows us to easily prepare GHZ states using up to eight qubits. Numerically optimized envelopes allow for even more precise quantum gate protocols applied to longer atom chains [17].

1.3 Qubit implementations

To encode qubits to Rydberg atoms' energy level we can choose various settings [13]. While we choose to use exclusively one type of qubit encoding, it's right to briefly introduce the other general ways to encode qubits using Rydberg atoms.

A possibility is the so-called rr'-qubit, encoded by setting the $|0\rangle$ state to a Rydberg level $|r\rangle$, while the $|1\rangle$ state is associated with another Rydberg state, $|r'\rangle$[3]. This configuration is the most convenient for obtaining different types of interactions, like short-ranged van der Waals interactions and longer-range dipolar-exchange interactions in the form $\frac{C_3}{R_{ij}^3}(|10\rangle\langle 01| + |01\rangle\langle 10|)$. This method proves itself to be optimal for implementing less-trivial geometric atom configurations like staggered atom chains [18].

Another very promising possibility is the gg'-qubit. It has recently been proven to be a good platform for implementing high-fidelity two-qubit controlled phase gates (99.5% fidelity with up to 60 atoms). For this reason, this method allows us to reliably prepare long-lived entangled states, as well as offer a new approach for the exploration of large-scale quantum error correction [19].

1.4 Experimental apparatus

The whole experimental setup is comprehensive of many elements. Despite its detailed description would be beyond the scope of this thesis, an overview of the typical setup is paramount.

[3] An example of atomic states in this case are $53S_{1/2}$ and $53P_{3/2}$ for $|r\rangle$ and $|r'\rangle$ respectively [13].

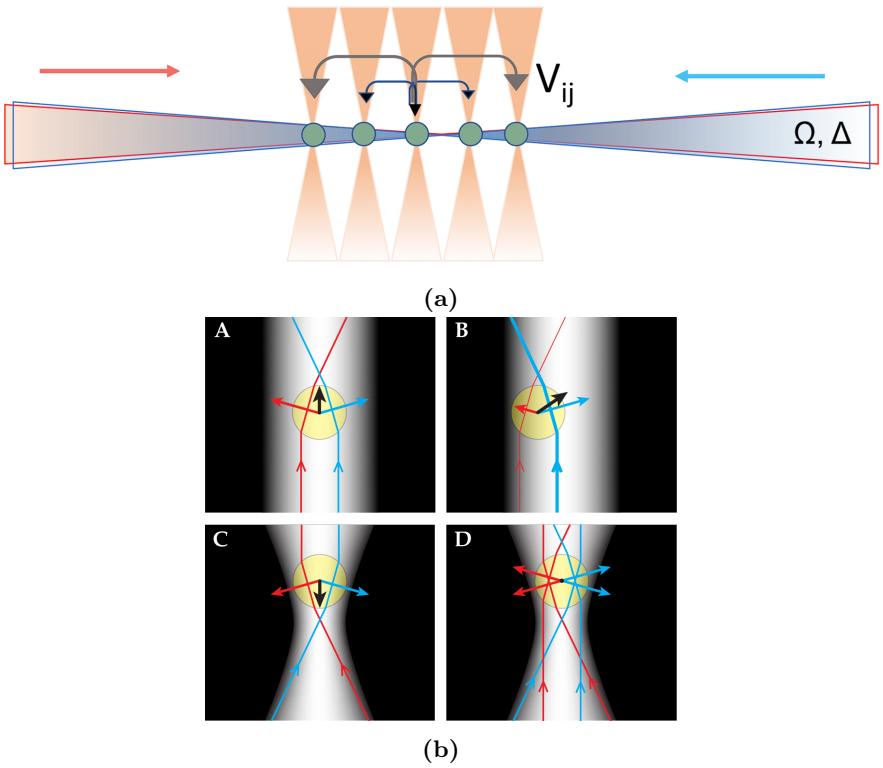

Figure 1.1: (a): Simple schematic of the system in exam; horizontal beams are the drive lasers, that carry signals for Ω and Δ. Vertical beams represent optical tweezers laser beams. In the figure are indicated interactions between the central atom and the neighboring ones, called V_{ij}. *Source:* [20]. (b): Operating principle of the tweezer traps. From A to C are displayed various positions where the atom experiences a non-zero net force, resulting in a displacement towards the equilibrium region (D). *Source:* [21].

First of all, the atom array is held in position by an array of optical tweezers, a useful instrument that uses a highly focused laser to hold and move atoms in the size range of μm. In Rydberg atom chains, atoms are loaded and held into their designated positions in an array constructed by an acousto-optic deflector (AOD), which splits a single laser beam in an array of optical tweezers. The trap itself consists of a laser beam; each atom is trapped at the narrowest part of the focused beam. This is because, at the beam waist, the focused laser creates a very strong electric field gradient, with the region with the strongest field being at the center of the waist, as shown in Fig. 1.1b. The particle is, more precisely, positioned slightly off the center of the waist, due to the particle interacting with the photons, which are scattered or absorbed by the particle.

However, interactions between the focused laser and the atoms are inevitable when the tweezer system is at work; thus to apply quantum manipulation of the states, the traps are turned off for not more than a few microseconds. In this timeframe, lasers are pulsed throughout the atom chain, realizing the effective Hamiltonian and implementing the time evolution.

To perform a measurement after a protocol has ended, the traps are turned on again. Atoms in the ground $|g\rangle$ state are recaptured, while the ones in the Rydberg state $|r\rangle$ are pushed away; the long lifetime of these excited states ensures that most of the Rydberg atoms can escape the traps before decaying back to the ground state. This conveniently allows us to measure the atomic state of every component of the array, by checking which trap sites are empty. Usually, fluorescence imaging is exploited to measure the array before and after the protocol, to compare the initial and the final state of the array [14].

Chapter 2

Qruise simulation software

For the numerical simulations, we use software provided by the company Qruise. This toolkit allows us to test experimental protocols, simulating the principal components of the system; it also provides extensive information about the system, which can be easily accessed by specific modules. The software consists of a collection of modules that are comprehensive of several system-optimized libraries with dedicated objects for every component of the experimental apparatus.

In this chapter, we describe the standard procedures we used to achieve our results, displaying the principal packages Qruise is equipped with to implement a faithful simulation of Rydberg atom arrays. Moreover, we test how far classical simulation software can be pushed to reproduce complex quantum dynamics.

2.1 General description of Qruise

Qruise is a Python-based collection of packages that allows us to create a virtual twin of a real experiment, with the aim of accelerating the development of quantum technology and improving its application.

The company offers space on its servers to store the user's file system and to remotely run code. To implement these features, the default interactive development environment (IDE) is Jupyter Notebook, which offers a dynamic way to write code and to make it human-accessible, with the aid of cells that run code or serve as markdown text.

Once the appropriate libraries have been imported, we can set up every component necessary to emulate our system. Then we can create objects that store parameters given by our component settings, and that compute the Hamiltonian terms.

Qruise methods make use of a class named `Quantity` to define physical quantities, in which we can specify their measurement unit, their numerical value, and if needed, the range of values it can vary. Once the experiment is created, running the simulation makes the computer integrate the related Schrödinger equation and the system's time evolution.

This allows us to explore dynamics, providing an initial state, of our virtual setup. For instance, when considering a chain of two-level systems, we can compute the time-evolution of a given initial state, that is the probability after a time t of measuring each state of the computational basis $B = \{(1,0,0,\cdots,0,0),(0,1,0,\cdots,0,0),\cdots,(0,0,0,\cdots,0,1)\}$, where $(x_1, x_2, \cdots, x_{2^n})$ is a 2^n-long vector indexing a specific configuration of the atomic excitations in the array.

2.2 The `rydberg` library

A convenient feature of the software is the possibility of selecting the specific physical hardware to simulate via a proper library: in this thesis, we use `rydberg`, which is a library containing classes and methods specifically intended to characterize Rydberg atom arrays.

```
#Rabi pulse params
omega_max = 5 * 2 * np.pi
t_rise=2.1e-6
t_fall=2.1e-6

#detuning params
delta_0 = -10.0 * 2 * np.pi
delta_f = 7.5 * 2 * np.pi
t_d_rise = 0.0e-6
t_d_fall = 0.0e-6

#gate time
t_gate_final = 15.0e-6

#simulation time
t_final = t_gate_final

vdW_coeff = 10840317060000.000
blockade_radius = ((vdW_coeff)/(2*np.pi*omega_max*1e6))**(1/6)

# of atoms
qb_number = 6

spacing = blockade_radius * 0.85

hilbert_dim = 2
```

Figure 2.1: Definition of parameter values, needed to define signals and array properties.

```
qb_pos_list = []
qb_name_list = []

for i in range(qb_number):
    qb_pos_list.append( i * spacing)
    name_entry = "Q" + str(i)
    qb_name_list.append (name_entry)


lattice = FromCoordinates(qb_pos_list, spacing) #Method used to create an array of atoms

rydsys = RydbergSystem(lattice=lattice, hilbert_dim=hilbert_dim) #RydbergSystem object

rydsys.sim_res = 5.0e8 #resolution of the simulation
```

Figure 2.2: Definition of the atom array, in which we can define various objects throughout the code. For the `FromCoordinates` method, an array of atom positions has to be created. The `RydbergSystem` method creates the mainframe for each object to interface with the simulation; the simulation resolution is defined by the method `.sim_res`.

We first initialize the parameters needed for the simulation (Fig. 2.1). In this example, `omega_max` is the height of a trapezoidal impulse, in MHz, while `t_rise` and `t_fall` the times

in µs the signal goes from zero to `omega_max` and vice versa. `delta_0` and `delta_f` are the initial and final values of the detuning signal, in MHz, which is a linear ramp; `t_d_rise` and `t_d_fall` are the times, before and after the linear ramp, where the signal remains constant. `t_gate_final` and `t_final` represent respectively the duration of the gate and the simulation, both in µs. `vdW_coeff` is the value of the van der Waals coefficient C_6, with which we calculate the blockade radius. Last, `qb_number` is the number of atoms in our array, while `hilbert_dim` is the dimension of the single atom's Hilbert space[1].

Once these parameters are initialized, we can define the atom array, creating a list containing all the positions of the atoms, with distances expressed in micrometers, and pass it to a method called `FromCoordinates`; the result is stored as a `Lattice` object. We can store this in an object created by the `RydbergSystem` instance, as shown in Fig. 2.2, and add components along the way; these components include the drive pulses and the virtual generator of these signals, which converts mathematical definitions of the signals to laser pulses.

Regarding the numerical simulation, we then can define the simulation's resolution, which is going to impact the length of the timestep, and the propagation method for the numerical integration of the Schrödinger equation.

Definition of the signals

```
#Amplitude drive
rydsys.add_drive("amplitude", "amplitude_afm_array", connected=qb_name_list,)
#Detuning drive
rydsys.add_drive("detuning", "detuning_afm_array", connected=qb_name_list)
```

```
##### Trapezoid envelope
scalene_trapezoid_amplitude_params = {
    "amp": Quantity(value=omega_max, min_val=-0.1, max_val=10 * 1e6, unit="V"),
    "slope_factor": Quantity(value=1.0),
    "rise": Quantity(value=t_rise),
    "fall": Quantity(value=t_fall),
    "t_final": Quantity(
        value=t_gate_final, min_val=0.9 * t_gate_final, max_val=1.1 * t_gate_final, unit="s"
    ),
}

scalene_trapezoid_amplitude = pulse.Envelope(
    name="amplitude",
    desc="Scalene trapezoid envelope for amplitude",
    params=scalene_trapezoid_amplitude_params,
    shape=envelopes['scalene_trapezoid'],
)
```

Figure 2.3: Example of a definition of one envelope, with its parameters. The general shape of the envelope is picked from an extensive list present in Qruise documentation.

Next, we have to provide our system with drives through which the signals are applied, using the method `add_drive`. We can then define the envelopes of the signals, choosing from an exhaustive list of pre-coded mathematical functions, and fine-tuning them to specify their parameters (Fig. 2.3).

[1] In our case the atom is considered a two-level system, with state space spanned by $|0\rangle$ and $|1\rangle$ states.

```
v2Hz = 1e6
simplegen = SimpleGenerator(
    V_to_Hz=Quantity(value=v2Hz, min_val=0.9*v2Hz, max_val=1.1*v2Hz, unit="Hz/V")
)
rydsys.set_generator(simplegen)
```

```
rydsys.clear_instructions()

single_instr_1 = gates.Instruction(
    name="GHZ_signal",
    t_start=0.0,
    t_end=t_gate_final,
    channels=["amplitude_afm_array", "detuning_afm_array"],
)

rydsys.add_instruction(
    single_instr_1,
    [scalene_trapezoid_amplitude,linear_ramp_detuning],
    ["amplitude_afm_array", "detuning_afm_array"]
)
```

Figure 2.4: Definiton of a virtual generator, that converts instructions to signal definition, once an envelope is provided by the `.add_instruction` method.

To do so, we have to create a generator object, which will provide the signals to the system through instructions. When defining these instructions with the `gates.Instruction` method, we have to specify the time window in which they have to be performed, as well as which drives the signals have to be provided to (Fig. 2.4).

```
rydsys.create_model()
rydsys.create_experiment()
rydsys.run()
```

```
rydsys.parameter_map.print_all_parameters()
```

```
dynamics_data = rydsys.experiment.dynamics(['GHZ_signal'], comp_basis[init_state_index])
```

Figure 2.5: On first cell, instructions to run the simulation and create the objects to store data; on second cell, the main method to retrieve parameters of the simulated system (`print_all_parameters()`); on third cell, the main method used to retrieve data after the simulation: the output stored in `dynamics_data` is a matrix of complex numbers: every line of the matrix, correspondent to a timestep, contains the probability amplitude of every state in the computational basis.

Finally, we can collect all the objects to define our experiment and run a simulation for the specified time. This is going to numerically solve the equations and provide us with the time evolution of the system, with which we can inspect the dynamics of an initial state (Fig. 2.5).

Before we can talk about simulations, we have to briefly see how the atoms are defined in Qruise, to implement a given protocol.

First of all, the various atoms are defined as `component` objects in the `RydbergSystem` library, where one can customize the relevant properties of our atoms, like the energy levels of the various Rydberg states. We use the default parameters for the virtual atoms in use; this poses no issue, since Qruise's framework conveniently stores all parameters of the simulation, giving us access to a variety of useful information, such as the van der Waals interaction coefficient C_6.

Regarding the various signals applied through the drive channels, they are defined as voltage functions, called `envelopes`. Then depending on the user-defined generator conversion factor Γ, they will be translated into the needed frequency. For instance, if we want to set a rectangular signal for Ω to $5 \times 2\pi$ MHz, we have to first define a voltage function $\Phi(t)$ shaped as a rectangle, where its height is $5 \times 2\pi$ V, and then pass this envelope as an instruction for the generator, which in the simplest setting reproduces our signal without noise, converted by a factor $\Gamma = 1.0$ MHz/V.

2.3 Limitations of the software

While Qruise is a user-friendly simulation software, it shows limitations, due to the exponential complexity of the simulations; this is because the simulations are based on exact diagonalization techniques. We briefly want to examine our issues regarding the capabilities of reproducing larger arrays, because they constitute the limit on what systems we are going to take results, on while keeping in mind that we are using a classical approach to simulate quantum systems.

Our issues can be divided into three categories:

- For the scope of our thesis, given the exact diagonalization method, we are limited to the size of the array. In our runs, we encountered issues that can divided into three categories: faithfulness of the simulations, crashes, and difficulties to implement features. These points ultimately impact precision on iterative methods, forcing us to do less defined or more narrow-ranged iterations over parameters.

- The faithfulness of our simulations depends on the choice of the proper propagator: with unitary methods like Piecewise Constant, we ensure the norm preservation. Using this method implies that, for each timestep, the simulation calculates the next unitary evolution operator, which is a matrix exponential; this method thus is slower, but more accurate, than others like Runge-Kutta. The latter one is much faster because the simulation calculates for each timestep the state as a multiplication between the previous state vector and a constant matrix. However this doesn't preserve the norm of the state vector over time, thus the Runge-Kutta method is avoided for our simulations.

  The resolution of the simulation, which is related to the length of the timestep, can be tuned to partially mitigate the duration of our simulation.

- Kernel crashes, which completely halt the simulation, are probably caused by the cloud framework and could be solved by running the entire software locally. This problem occurs frequently on nine or more atoms, making it impossible for us to do iterative runs on more than eight atom arrays, or simulate the dynamics of a high number of atoms.

- Last, the Qruise suite offers documentation and tutorial scripts about its software; however, from a new user perspective, we find that some modules like `RydbergAtoms` lack some key informative material to correctly implement the needed experimental features.

Chapter 3

Preparation of the GHZ state

In this chapter, we show and discuss our simulations and the results we obtained.

First, we focus on a global not-gate that flips all the atoms from $|0\rangle$ to $|1\rangle$. This was performed as a control run, to better familiarize with the software as well as quantitatively assert the dynamics of the system in a simple and predictable setting.

Then, to explore how the Rydberg blockade impacts on the array's evolution, we simulate how a system of n atoms behaves when the atoms are put close to each other. In this case, we can observe that the probability of a single atom excitation oscillates between 0 and 1, with frequency equal to the Rabi frequency multiplied by $\sqrt{n}$, while multiple excitations are highly suppressed. In this instance, we also checked how introducing a detuning term affects the dynamics.

Finally, taking inspiration from [14], we reproduce the protocol to prepare the GHZ state. We explain how the detuning values and the array spacing, are crucial factors in the preparation of the GHZ state.

3.1 NOT gate implementation

As exposed above, we start our analysis by preparing a simple script that reproduces collective oscillations between the states $|0000\rangle$ and $|1111\rangle$. We firstly make sure that our atoms are not interacting with each other by setting the spacing $a \gg R_b$; we found that setting $a = 20\mu\text{m}$ enforces this condition, given that $R_b \simeq 6.17\mu\text{m}$. Then, we define a Rabi pulse trapezoid signal, as shown in Fig. 3.1, where the length of the bottom base of the trapezoid is the gate time t_g, and its height is the Rabi frequency Ω.

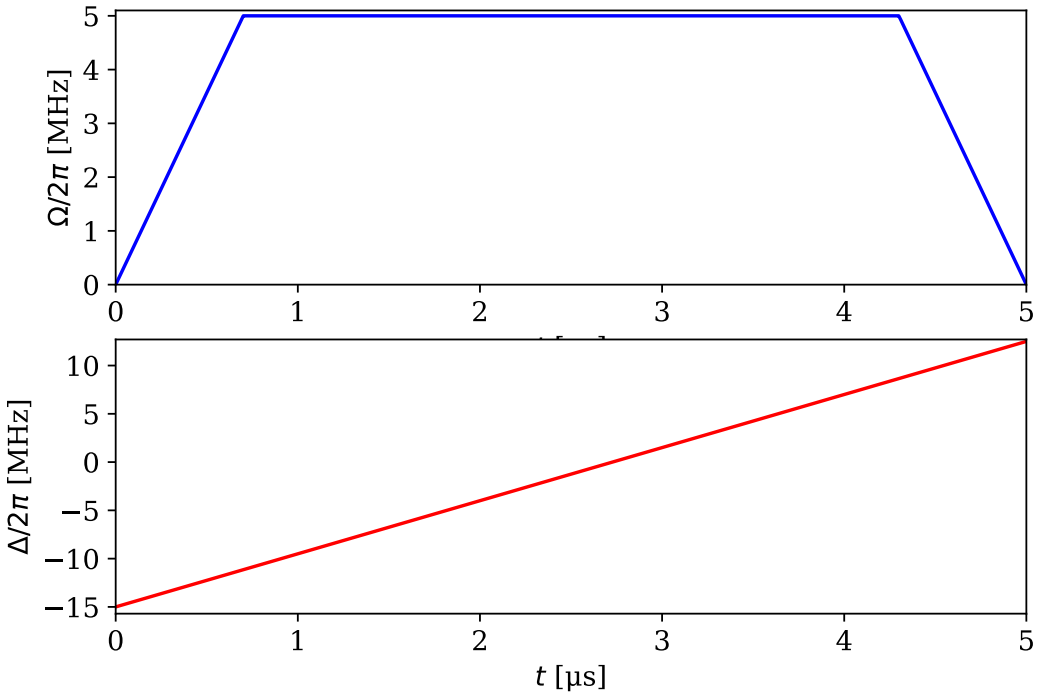

Figure 3.1: Envelopes carried by the generator. Regarding the linear ramp, the final value of Δ varies over iterations from $7.5\times 2\pi$MHz to $12.5\times$MHz, while the initial value is fixed at $\Delta_i = -15.0\times 2\pi$MHz; maximum amplitude for $\Omega(t)$ is $\Omega_{max} = 5.0 \times 2\pi$MHz; $\Omega(t)$ rises or falls between 0 and Ω_{max} in $t_{risefall} = 0.7\mu$s.

As seen before, if the atoms are sufficiently far away from each other they are not interacting, so the unitary evolution operator takes the form

$$U(t_g) = \cos\big(\phi(t_g, t_{on})\big)\mathbf{1}_2 - i\sin\big(\phi(t_g, t_{on})\big)\sigma_x, \tag{3.1}$$

where t_g and t_{on} are respectively the bottom and upper base of the trapezoid signal, and $\phi(t_g, t_{on}) = (t_g + t_{on})\Omega/2$, obtained as the underlying area of the trapezoid; so if we want to perform a global NOT gate we simply have to adjust the length of the two bases of the trapezoid, and Ω, to suppress the cosine term.

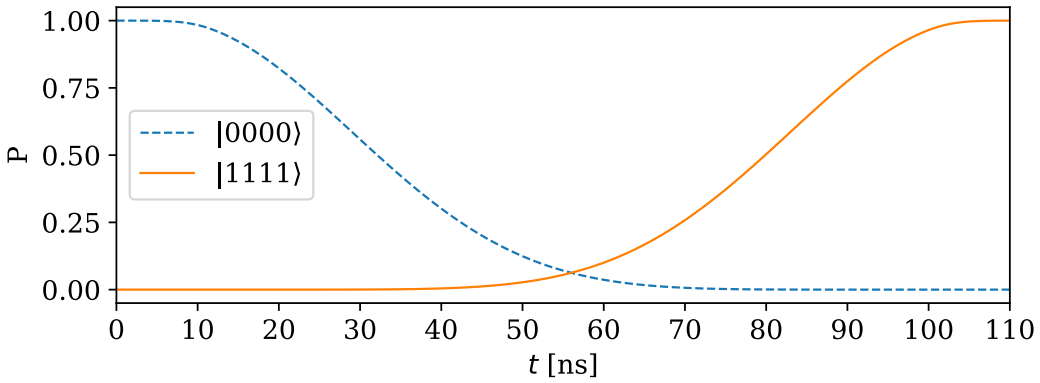

(a)

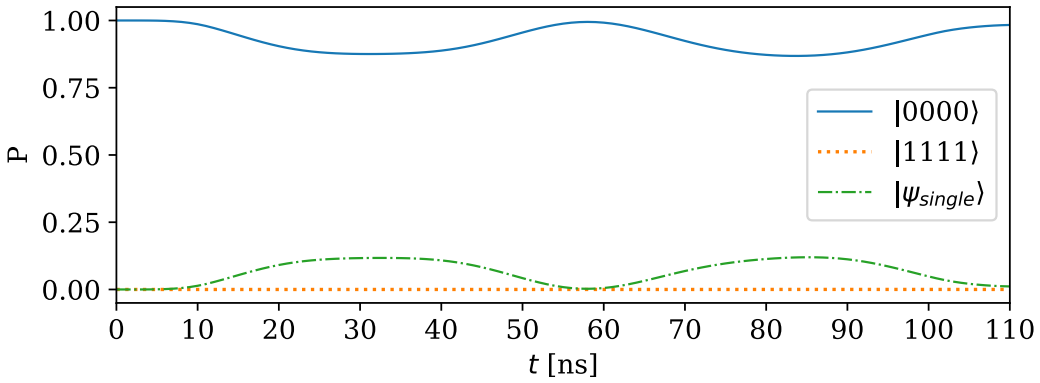

(b)

Figure 3.2: Constant amplitude Ω signal applied to an array of four atoms, where site spacing is 20µm in (a), and 6.0µm in (b). The fact that the $|0000\rangle$ curve on (b) is not constant is due to single-excitation states ψ_{single}, having the remaining probability. Simulations shown here are of a 4-atom array, with trapezoidal pulse $\Omega(t)$ with a max value of $\Omega(t)/2\pi = 5.0$MHz, and $t_{on} = 90$ns, over a time of 110ns.

The simulation performed implements a gate time $t_g = 110$ns, while the upper basis of the trapezoidal envelope is $t_{on} = 90$ns; maximum amplitude is set as $\Omega/2\pi = 5$MHz. The spacing between atoms is set big enough to neglect van der Waals interactions; that implies that the dominant term of the Hamiltonian is the one that applies σ_x^i to every qubit.

As shown in Fig. 3.2a, the initial state is the $|0000\rangle$ state. Its probability decreases over time as the Ω pulse is applied, and after the time t_g the state is the one with all atoms excited, $|1111\rangle$: the probability fully transfers between these two states because they have the same energy. Then, we test the behavior of the system by setting $a = 6.0\mu\text{m} \simeq R_b$, like 3.2b clearly shows, resulting in the transition from $|0000\rangle$ to $|1111\rangle$ to be forbidden because the energy of the initial state is zero, while the energy of $|1111\rangle$ is $\gg 0$. The interaction energy is increased, since it is the dominant term, due to the atom spacing. In this case, the $|1111\rangle$ state is highly suppressed.

3.2 Single excitation oscillations

Our next goal is to verify how the initial state would evolve if the lattice spacing is diminished such that $(n-1)a < R_b$, namely when the atoms are simultaneously subjected to the Rydberg blockade. In this regime, we expect that, during the dynamics, no more than a single excitation

will emerge since the Rydberg blockade effect is going to suppress every couple of double excitations in the lattice.

However, we also expect that the total probability of having exactly one atom excited is shared across all the states with a single excitation, that is states such as $|x_i\rangle^{\otimes n}$ where $x_i = 1$ for $i = i^*$ and $x_i = 0$ for every other i. This is because there is translational invariance across the array, and every state with a single excitation has energy $E > 0$; this means that these states are all resonant with the initial state. We observe oscillations between the initial state and the state

$$|\psi_s\rangle = \frac{1}{\sqrt{n}}\big(\,|1000...\rangle + |0100...\rangle + ... + |...0001\rangle\,\big), \tag{3.2}$$

as already discussed in chapter 1.2.

We set our pulse to be carried by a uniform and constant envelope of amplitude $\Omega = 2.5 \times 2\pi$ MHz and duration 1.2µs; to be sure that every atom is in every other's blockade radius, we set the array spacing as $a = \frac{R_b}{n+1}$, with $R_b \simeq 6.17$µm.

We evolve the system for a time such that we observe several oscillations.

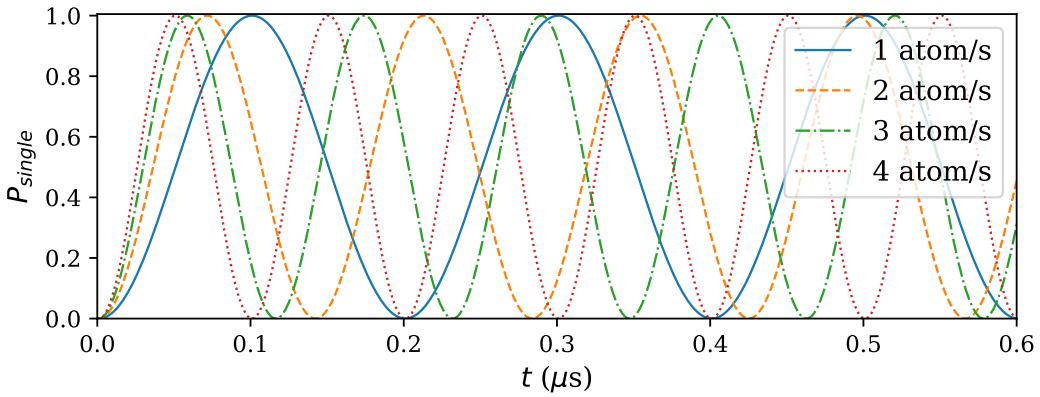

(a)

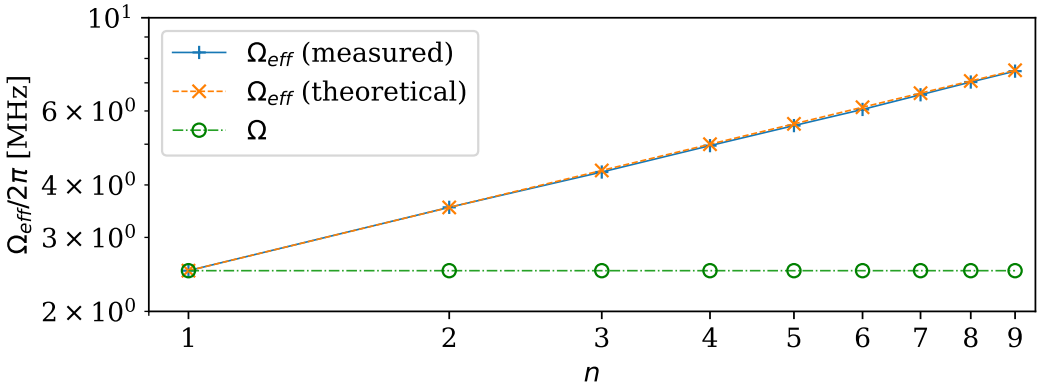

(b)

Figure 3.3: (a) Various oscillations of the single-atom excitation probability P_{single}, depending on the number of atoms n. Only 0.6µs of simulation are shown to avoid visual clutter.
(b) Measured oscillation frequencies of arrays of n atoms, compared with theoretical expected values (Ω_{eff}(theor.)) and the Rabi frequency (Ω). We have to note that, albeit useful to verify the frequency relation, the 9-atom acquisition is not physically suitable on real systems that possess our value for the blockade radius, due to how close the atoms are in our array.
For both (a) and (b) we set a pulse of amplitude $\Omega/2\pi = 2.5$MHz.

We take the single-atom probability P_{single} as the sum of the populations of every state in Eq. 3.2.

As shown in Fig. 3.3a, as we increase n, the frequency of these oscillations increases. What we expect is that this frequency is proportional to $\sqrt{n}$, as predicted in chapter 1.2. To verify this prediction, we performed simulations up to nine atoms and measured the oscillation frequency by taking the inverse of the time where we have two peaks of the probability of $|\psi_s\rangle$, to confront them with their respective expected value from the theory, $\Omega_{eff} = \Omega\sqrt{n}$.

Fig. 3.3b confirms our predictions, showing almost exactly matching values between Ω_{eff}(measured) and Ω_{eff}(theoretical).

In any case, given our measure for R_b, estimations of the effective Rabi frequency on eight or nine qubits have to be taken only as a verification of the $\Omega_{eff} = \Omega\sqrt{n}$ relation, since the consequent atom spacing is unattainable in an experimental environment.

A final analysis of this virtual setup was performed, introducing a constant detuning Δ on every site. Since the Hamiltonian is time-independent, we expect that the system's energy is conserved, so we observe oscillations between states with resonant energies. As a result, when detuning is not present, the system's state probability fully transfers from $|\psi_g\rangle$ to $|\psi_s\rangle$, ranging from 0 to 1. However, when introducing a detuning $\Delta > 0$, this probability shift is partially suppressed, resulting in a reduction of the amplitude of the $|\psi_s\rangle$ probability oscillations. This results can be visualized in Fig. 3.4:

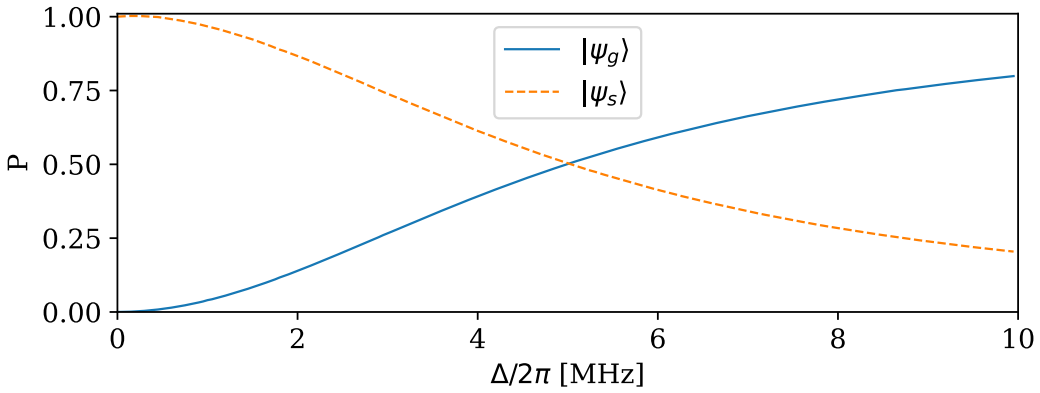

Figure 3.4: Probability shift from $|\psi_s\rangle$ to $|\psi_g\rangle$. The dashed line indicates maximum values of probability oscillations of $|\psi_s\rangle$, while the continuous line shows minimum values of $|\psi_g\rangle$ while varying the detuning value on all 4 sites. Simulation parameters are: $t_{gate} = 1.2\mu s$, $\Omega/2\pi = 5.0$ MHz, $a = \frac{R_b}{n+1}$

3.3 GHZ states preparation

Finally, we want to set up a protocol to obtain a GHZ state, defined as the coherent superposition of the two antiferromagnetic states:

$$|\psi_{GHZ}\rangle = \frac{1}{\sqrt{2}}\big(\,|1010\cdots10\rangle + |0101\cdots01\rangle\,\big). \tag{3.3}$$

We focus only on even-numbered atom arrays because in this case, the two states that constitute the GHZ state have the same energy. If not specified, we set $n = 6$, but we have obtained analogous results for $n = 8$.

The simulations are performed with a total time of 5.0μs. The total duration is the same adopted in the experiment reported in [1]. Also, the initial state is $|00\cdots0\rangle$.

We set a trapezoid profile for the Rabi pulse and a linear ramp for the detuning one, as shown in Fig. 3.1:

Depending on the spacing a and the final value of the detuning Δ_f, we observe different probabilities for the GHZ state:

- If a and Δ_f are set to be too low ($a < 0.65R_b$, $\Delta_f/2\pi < 5.0$ MHz), the interaction term is the dominant one, resulting in less than $\frac{n}{2}$ excitations due to the blockade mechanism;
- If $a \gtrsim R_b$, we will have the opposite phenomena, namely blockade violations, resulting in more than half of the atoms excited. These states are furthermore populated with the presence of higher values of Δ_f;
- In the cases where only half the atoms are excited without violating the blockade, the possible states have all similar energy. For example, considering an array of four atoms for brevity, the most probable final states are $|1010\rangle$, $|0101\rangle$, and $|1001\rangle$. The only state with both borders excited (BE state), namely $|1001\rangle$, is the most probable one. This is expected, since the first and the fourth atoms experience weaker interactions, having only one neighboring atom. As a result, the BE state has less energy compared to the other two.

Using this reasoning, for the third case we choose to search for the optimal combination of parameters by spanning a range of values of a and Δ, to prepare final states with only $n/2$ atoms excited without blockade violations. However, a local correction on the Δ signal is implemented on the border atoms, to mitigate the presence of BE states, and instead promote the formation of the GHZ state. The final value, and thus the slope, for the detuning signal, now depends on the site, starting from the same value for all atoms but ending, for the i-th site, at

$$\Delta_f(i) = \Delta_f + \Delta_b(\delta_{1,i} + \delta_{i,n}). \tag{3.4}$$

If $\Delta_b > 0$, the final value of the detuning at border sites is higher in modules, resulting in a higher probability of BE-states.

If instead, we choose $-\Delta_f < \Delta_b < 0$, we increase the energy of the undesired states, thus we reduce their probability in the final state. Therefore we increase the probability for a GHZ state, since interatomic interactions are weaker at border sites, and applying a smaller value of the detuning on these atoms results in less probable BE states.

If $\Delta_b < -\Delta_f$, we suppress the effect of detuning, reducing the probability of finding the $n/2$-excitations states.

We run a small number of iterated simulations, varying Δ_f and a/R_b at every iteration, and setting $\Delta_b = 0$. In this case, we observed the highest probability of having a GHZ as a final state to be inferior ($P_{GHZ} \sim 0.2$) to the highest probability of having a BE state ($P_{BE} \sim 0.8$). We then replicate the iteration runs; however, for every run, we now fix a constant value of $\Delta_b < 0$ and check the highest probability of having a final GHZ state at the specific values of Δ_f and a/R_b. We observe $P_{GHZ} \sim 0.9$ at $a = 0.85R_b$ and $\Delta_f/2\pi = 7.5MHz$.

Keeping fixed these optimal values of Δ_f and a/R_b, we perform another iteration, sweeping Δ_f/Δ_b from -1.0 to 0.0, as shown in Fig. 3.5.

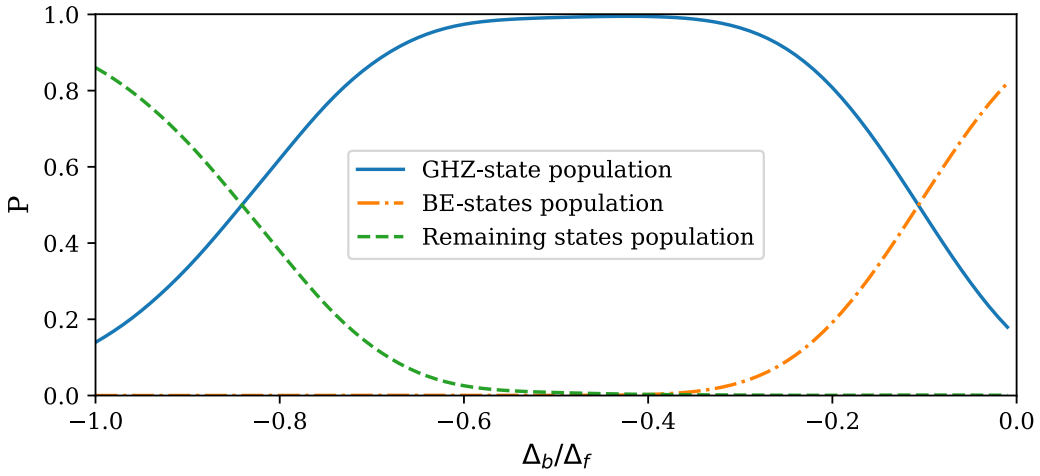

Figure 3.5: Populations of the various 6-atom states, when decreasing the final detuning value at the borders by Δ_B, with spacing $a = 0.85R_b$ and final detuning $\Delta_f/2\pi = 7.5$ MHz. As we discussed, the presence of Δ_b is necessary to obtain GHZ states with good probability: if the detuning slope is equal for all sites ($\Delta_b = 0$), BE-states probability (~ 0.8) is much greater than the GHZ-state one (~ 0.2).

As we can see from Fig. 3.5, the population of the GHZ state decreases the more we approach $\Delta_b = 0$, which is uniform detuning for all atoms. Instead, if $\Delta_b = -\Delta_f$, we are forcing both border atoms to not excite, resulting in less-than-$n/2$ excitations due to the Rydberg blockade. We also find the optimal values of Δ_b to be $\Delta_b \sim -0.4\Delta_f$.

Setting $\Delta_b = -0.4\Delta_f$, we perform two final sets of iterations, one for the six-atom array and one for the eight-atom one, sweeping the values of Δ_f and a/R_b. For each set, at each iteration, we extract the probability of having the GHZ state as the final state, spanning a grid of values of that probability, shown in Fig. 3.6 and Fig. 3.7.

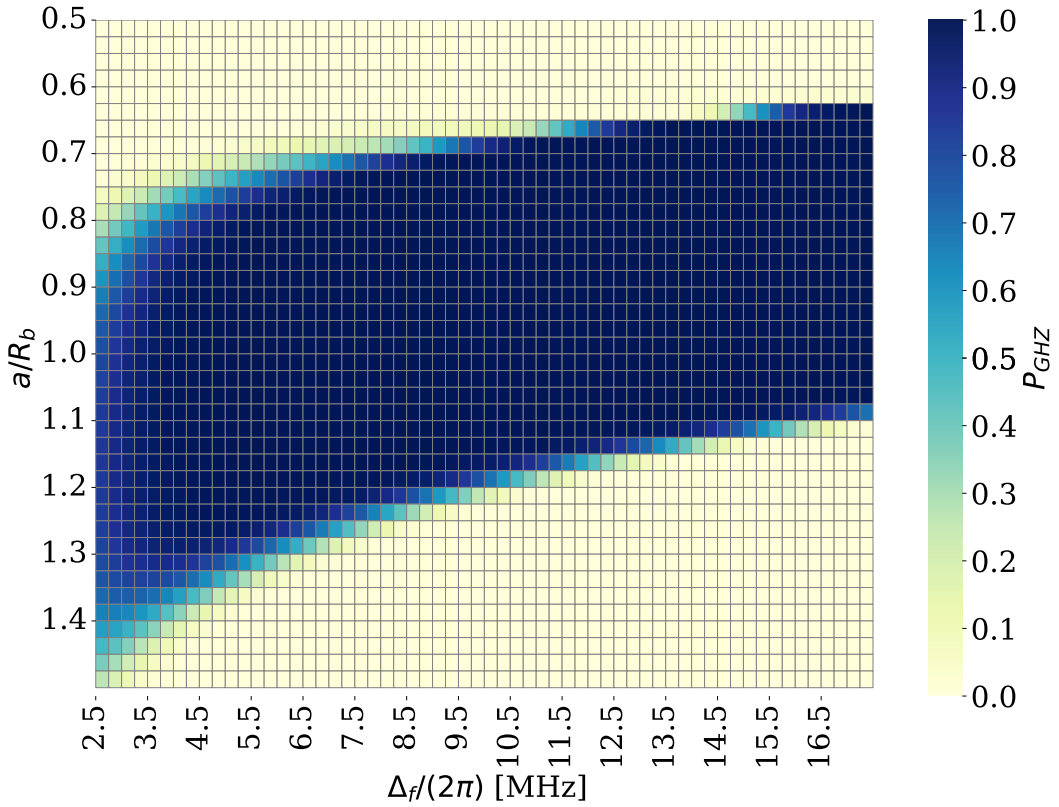

Figure 3.6: Heatmap showing the probability of the final state to be measured as one of the two components of $|\psi_{GHZ}\rangle$, on an array of 6 atoms. This result is obtained iterating initial parameters a and Δ_f, while $\Delta_b/\Delta_f = -0.4$ is kept fixed. The best probability is found at $a/R_b = 0.825$ and $\Delta_f/2\pi = 16.75$MHz, with value $P_{GHZ} = 0.99995$.

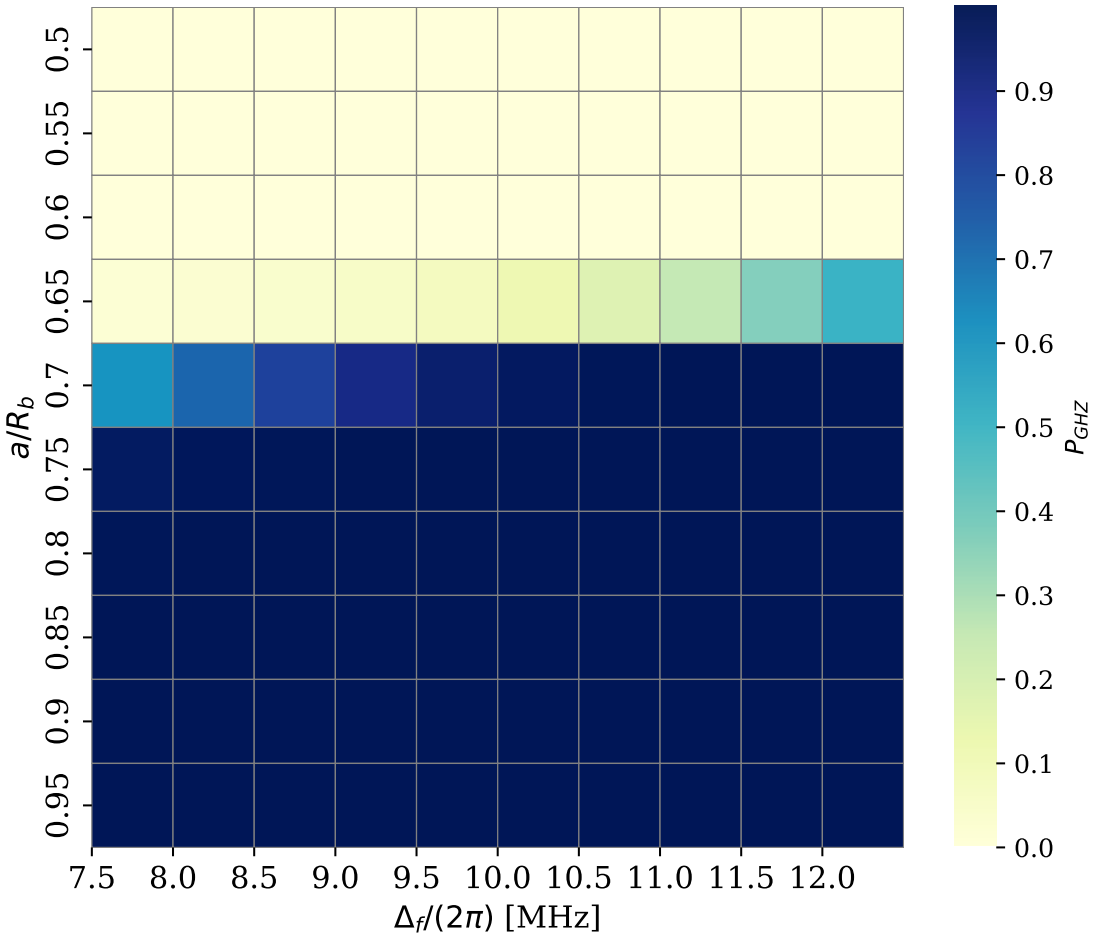

Figure 3.7: Heatmap showing the probability of the final state to be measured as one of the two components of $|\psi_{GHZ}\rangle$, on an array of 8 atoms. This result is obtained in the same way of Fig. 3.6, with a/R_b ranging from 0.5 to 0.95m, and $\Delta_f/2\pi$ from 7.5 to 12.0MHz, while keeping $\Delta_b/\Delta_f = -0.4$. Due to the limitations discussed in chapter 2.3, we have to decrease the range and the resolution of the heatmap. Nonetheless, good results are obtained, with best probability $P_{GHZ} = 0.9996$, found at $a/R_b = 0.95$ and $\Delta_f/2\pi = 9.0$MHz.

We find satisfying results for both the arrays:

For $n = 6$, the probability of having a final GHZ state has its maximum value $P_{GHZ} = 0.99995 \simeq 1$ with $a/R_b = 0.825$ and $\Delta_f/2\pi = 16.75$MHz. However, as already shown in Fig. 3.6, we have a belt of high probabilities. This means that similar values of P_{GHZ} are obtainable with multiple values of a and Δ_f.

We also notice that the belt trend is towards smaller values of Δ_f when a is higher: this has to be expected since the more a is increased, the more we have blockade violation, which is further incentivized at high values of Δ_f. For the opposite reason, at smaller values of a, we need higher values of Δ_f to lower the energy of 3-atoms-excited states, otherwise, due to the blockade, 2 excitation states are favored.

For $n = 8$, we have analogous results: $P_{GHZ} = 0.9996 \simeq 1$ with $a/R_b = 0.95$ and $\Delta_f/2\pi = 9.0$MHz (Fig. 3.7). Even if the range and resolution of the map are smaller than the six atoms case, we still clearly see that high values of P_{GHZ} can be obtained in a wide range of parameter values. The map also suggests that the belt trend in this case would be the same.

For both cases, we can assert that a relatively wide range of a and Δ_f values can be set

to obtain GHZ final states with ~ 1 probability, if we apply a local detuning correction to the border atoms.

Last, we provide an example of the dynamics of a GHZ state preparation protocol for 6 and 8 atoms in Fig. 3.8. The parameters in use here are the same for both cases.

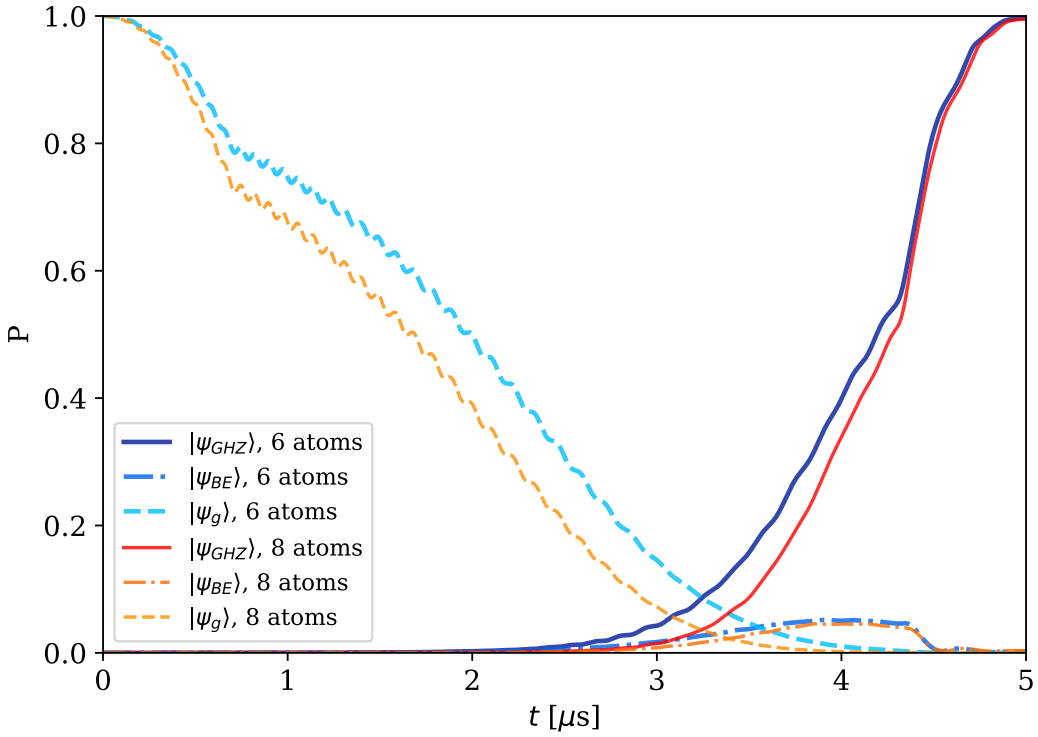

Figure 3.8: Probabilities as functions of time of the ground state, GHZ state, and the BE states. Parameters are: $a = 0.85R_b$, $\Omega_{max}/2\pi = 5.0$ MHz, $\Delta/2\pi = -15.0$ to 12.5 MHz, $\Delta_b/\Delta_f = -0.4$. In blue are shown the probabilities relative to an array of 6 atoms, while in red the ones of an array of 8 atoms.

Conclusions

In this thesis we have simulated the preparation of a GHZ state in a one-dimensional array of Rydberg atoms.

First, we have started by simulating a simple NOT gate, to test Qruise's core features and familiarize with how it simulates the system under a predictable environment. Then, we have explored how the various terms of the Hamiltonian affect the system's dynamics; considering the interatomic interactions between Rydberg atoms, we have reproduced the Rydberg blockade phenomena with multiple sites, confirming that the system we have simulated exhibits genuine quantum properties, such as the raising of the effective Rabi oscillations' frequency when more atoms are added in the blockade regime. Our results show us that the effect of the detuning is lowering the energy of multiple excitation states, resulting in an attenuation of the blockade effect.

Then, we moved to the generation of many-atoms superposition of entangled states, resulting in excellent results on recreating six and eight Rydberg atoms Schrödinger's cat states. To achieve this goal, we run the simulation iterating over multiple parameters choice, to find the optimal combination of them to maximize these states' populations.

We also have determined the importance of applying additional local detuning at the array's border sites, to diminish as much as possible the population of resonant states with both borders excited.

We hence have proven that Rydberg atoms optical lattices are not only a powerful candidate for quantum simulation and computation, but also a versatile one, given the various results we obtained by varying a few important parameters of our array.

In pursuing such objectives we also have shown that quantum simulators are a necessity for experimental research since the simulation of even a few atoms proved to be a computationally expensive task for our simulator; in our attempts not more than nine-atom simulations were successful, either due to the long run times or to precision errors from the calculations.

In summary, our exploration of the properties of Rydberg atom chains and their simulation using Qruise highlights the potential of neutral atom lattices for quantum simulation and computation. However, our thesis also underscores the need for further experimental endeavors to fully harness the capabilities of these systems to advance our understanding and application of quantum many-body systems.

Bibliography

[1] A. Omran et al., Science **365**, 570 (2019).

[2] R. P. Feynman, International Journal of Theoretical Physic **21**, 467 (1981).

[3] R. Blatt and C. F. Roos, Nature Physics **8**, 277 (2012).

[4] A. Blais and A. M. Zagoskin, Phisical review A **61** (2000).

[5] A. Aspect, Physics Reports **219**, 141 (1992).

[6] C. Cohen-Tannoudji, Physics Reports **219**, 153 (1992).

[7] P. W. Shor, SIAM Review **41** (1999).

[8] L. K. Grover, Physical review letters **95** (2005).

[9] B. A. Cordier, N. P. D. Sawaya, G. G. Guerreschi, and S. K. McWeeney, Journal of The Royal Society Interface **19** (2022).

[10] N. Herrman, arXiv:2303.02138v2[quant-ph] (2023).

[11] K. He et al., Chinese Physics B **30** (2021).

[12] B. Lanyon et al., Science **334** (2011).

[13] M. Morgado and S. Whitlock, Insitut de Science et d'Ingegnerie Supramoléculaires, University of Strasbourg and CNRS (2021).

[14] Bernien et al., Nature **551**, 579 (2017).

[15] T. F. Gallagher, *Springer Handbook of Atomic, Molecular, and Optical Physics* (Springer, 1998).

[16] C. S. Adams, J. D. Pritchard, and J. P. Shaffer, Journal of Physics B **53** (2019).

[17] J. Zoller, Ph.D. thesis, Open Access Repositorium der Universität Ulm und Technischen Hochschule Ulm (2018).

[18] S. de Léséleuc et al., arXiv:1810.13286[quant-ph] (2018).

[19] S. J. Evered, arXiv:2304.05420[quant-ph] (2023).

[20] J. Georgaras, Tech. Rep., Department of Physics, Stanford University, Stanford, CA 94305 (2020).

[21] J. F. Lindner, *Optical tweezers*, https://woosterphysicists.scotblogs.wooster.edu/2018/10/21/optical-tweezers/ (2018).